Current Science International
Volume: 15 | Issue: 01| Jan. - March| 2026

EISSN:2706-7920 ISSN: 2077-4435
DOI: 10.36632/csi/2026.15.1.1
Journal homepage: www.curresweb.com
Pages: 1-10

Hydrogen Adsorption on Manganese-Doped Carbon, Boron Nitride, and Silicon Carbide Nanocones: A Density Functional Theory Study

M. A. Al-Khateeb

Physics Department, Faculty of Education and Science, Taiz University, Taiz, Yemen

Received: 06 Jan. 2026 **Accepted:** 15 Feb. 2026 **Published:** 10 Mar. 2026

ABSTRACT

The quest for efficient hydrogen storage media persists as a pivotal bottleneck in the transition toward large-scale hydrogen-based energy infrastructures. In the present study, systematic density functional theory (DFT) calculations were executed via the Gaussian 09 software package to scrutinize the hydrogen adsorption phenomena on pristine and manganese-doped nanocones (NCs) comprising carbon (C), boron nitride (BN), and silicon carbide (SiC). By employing a rigorous computational framework, we evaluated the structural stability and electronic modulation of these nanostructures to determine their viability for storage applications. Our findings underscore the superiority of the Mn–$Si_{41}C_{34}H_9$–M2 configuration characterized by a 300° disclination angle which demonstrated an exceptionally robust interaction with molecular hydrogen. This specific system yielded a significant adsorption energy of -4.98 eV, accompanied by a pronounced dipole moment enhancement of 25.74 D, thereby indicating substantial surface polarization. Furthermore, the electronic landscape analysis revealed an ultra-narrow energy gap of 0.02 eV for the Mn-doped SiC nanocone, suggesting a highly reactive state that facilitates charge transfer processes. Natural Population Analysis (NPA) and molecular orbital insights indicate that Mn incorporation induces a localized electronic redistribution, creating potent catalytic sites for hydrogen binding. Comparative assessment confirms that Mn-doped SiC nanocones outperform their C and BN counterparts in terms of binding affinity, highlighting the indispensable role of transition-metal doping in fine-tuning the chemisorption characteristics. These results provide critical theoretical benchmarks for designing dopant-induced nanoscale platforms tailored for high-capacity hydrogen storage.

Keywords: Hydrogen storage, carbon nanocones, boron nitride nanocones, silicon carbide nanocones, manganese doping, density functional theory, hydrogen adsorption.

1. Introduction

The escalating consumption of fossil fuels and the consequent environmental degradation have necessitated the search for clean, sustainable, and environmentally friendly energy alternatives to replace conventional energy sources (El-Barbary and Al-Khateeb, 2021; El-Barbary, 2019; Sattler, 1995; Al-Khateeb and El-Barbary, 2020; El-Barbary and Kamel *et al.,* 2015; El-Barbary, 2016a; Alfieri and Kimoto, 2009; Iijima., 1991; Al-Khateeb and El-Barbary, 2026; Ewels *et al.* 2003; Gali, 2006). Renewable and alternative energy sources have thus become a focal point of extensive research (Al-Khateeb and El-Barbary, 2025; EL-Barbary, 2016b; Nikitin *et al.* 2008; EL-Barbary, 2016c; Yang *et al.* 2006; Zetterling, 2002; Zhu *et al.* 2009; Wu and Guo, 2007). Among these, hydrogen is regarded as an ideal energy carrier due to its high energy density and clean combustion byproducts (Matsunami, 2004; Garberg *et al.* 2008; El-Barbary *et al.* 2015; Harris, 1995; Liu and Cheng, 2005; Telling *et al.* 2003). However, as highlighted by the United States Department of Energy (DOE), hydrogen storage remains a significant technological challenge. The DOE has established that a hydrogen storage density of 9 wt% (weight percent) is required to enable the widespread adoption of fuel-cell vehicles as a replacement for petroleum-fueled vehicles. The wt% is defined as the ratio of

Corresponding Author: M. A. Al-Khateeb, Physics Department, Faculty of Education and Science, Taiz University, Taiz, Yemen .
E-mail: m_alkhateeb77@yahoo.com, m_alkhateeb@taiz.edu.ye

the mass of stored hydrogen to the total mass of the storage system (Hindi and El-Barbary, 2015; Chen *et al.* 2023; Zeng *et al.* 2024). Hydrogen can be produced through various chemical reactions and stored in multiple forms, including liquid hydrogen, solid-state storage, and compressed gas. However, these methods often involve high pressures, bulky infrastructure, and relatively low storage efficiencies.

Nanomaterials have emerged as promising candidates for hydrogen storage due to their lightweight nature, cost-effectiveness, chemical stability, and favorable hydrogen adsorption and desorption properties. In particular, nanocones (NCs) have attracted attention due to their high chemical reactivity, which is attributed to the presence of nano windows at their tips or sidewalls (Strobel *et al.,* 2006; Jaramillo *et al.,* 2021; Pakhira and Mendoza-Cortes, 2019; Al-Khateeb and El-Barbary, 2018; Chen *et al.* 1999).

Manganese (Mn), a transition metal with atomic number 25, is known for its diverse oxidation states and catalytic properties. It is widely utilized in various applications, including batteries, catalysts, and as an essential trace element in biological systems (Wu *et al.,* 2022; Savini *et al.,* 2007; Yang and Yang, 2002; Suarez-Martinez *et al.* 2007; Kotz *et al.* 2006; Dongjie Shi *et al.,* 2022; Zhao *et al.,* 2005; El-Nahass *et al.,* 2013; Shalabi, *et al.,* 1998). Due to its unique physical, chemical, and biochemical characteristics, manganese plays a pivotal role in numerous industrial and biological processes, making it a subject of significant interest in fields such as catalysis, biosensing, and environmental remediation.

While recent research on manganese-based nanomaterials has predominantly focused on quantum dots and manganese oxide nanoparticles, other potential applications, such as hydrogen storage and the development of novel manganese-doped nanomaterials like Mn-doped nanocones, have received less attention.

This study focuses on three types of nanocones: carbon nanocones (CNCs), boron nitride nanocones (BNNCs), and silicon carbide nanocones (SiCNCs), each with disclination angles of 60˚ and 300˚. These nanocones are further modified by doping with a manganese (Mn) atom and subsequent mono hydrogenation and we calculate the adsorption energy, energy gaps (Eg), highest occupied molecular orbitals (HOMO), lowest unoccupied molecular orbitals (LUMO), and surface reactivity of both pure and Mn-doped CNCs, BNNCs, and SiCNCs with disclination angles of 60˚ and 300˚. By investigating these properties, we seek to advance the understanding of Mn-doped nanocones as potential materials for efficient hydrogen storage.

2. Computational details

The mono hydrogenation of both pure and Mn-doped nanocones (NCs) was investigated using Density Functional Theory (DFT) with full geometry optimization. The calculations employed the Becke three-parameter hybrid functional combined with the Lee-Yang-Parr (LYP) correlation functional (B3LYP) (Vosko *et al.,* 1980; Becke, 1993), along with a standard basis set, as implemented in the Gaussian 09 W program (Frisch *et al.,* 2009). All computations were conducted using the Gauss View 5 molecular visualization program package (Dennington *et al.,* 2009). The systems studied included pure NCs, Mn-doped NCs, mono hydrogenated pure NCs, and mono hydrogenated Mn-doped NCs. Three types of nanocones were examined: carbon nanocones (CNCs), boron nitride nanocones (BNNCs), and silicon carbide nanocones (SiCNCs), each with disclination angles of 60° and 300°.

For BNNCs with disclination angles of 60° and 300°, two distinct models (M1 and M2) were considered, differing in the connectivity of the edge atoms. In model M1, the edges were connected via nitrogen atoms, while in model M2, the edges were connected via boron atoms (see Figures 1(a), 1(b), 2(a), and 2(b)). Similarly, for SiCNCs, two models (M1 and M2) were analyzed, where the edges were connected via silicon atoms in model M1 and carbon atoms in model M2 (see Figures 1(c), 1(d), 2(c), and 2(d)). The fully optimized geometries of the three types of nanocones with disclination angles of 60° and 300° are illustrated in Figures 1 and 2.

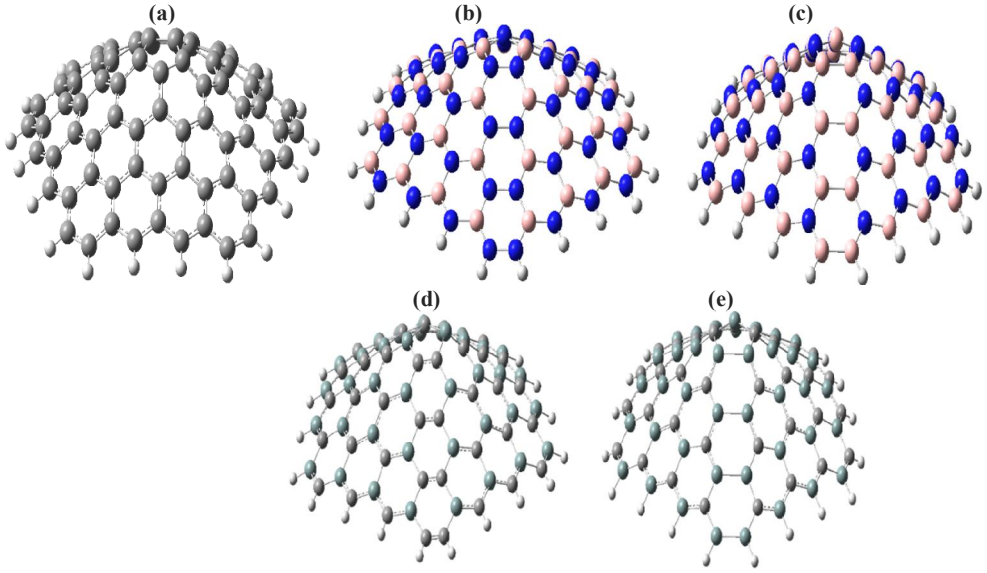

Fig. 1: The fully optimized structures of pure nanocones with disclination angle 60˚ **(a)** $C_{80}H_{20}$, **(b)** $B_{38}N_{42}H_{20}$-M1, **(c)** $B_{42}N_{38}H_{20}$-M2 (blue atoms represent nitrogen atoms and pink atoms represent boron atoms), **(d)** $Si_{38}C_{42}$ H_{20}-M1, **(e)** $Si_{42}C_{38}H_{20}$-M2 (dark cyan atoms represent silicon atoms and grey atoms represent carbon atoms).

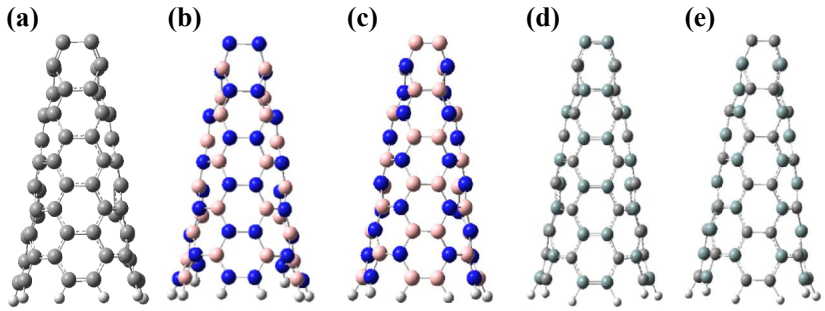

Fig. 2. The fully optimized structures of nanocones with disclination angle 300˚ **(a)** $C_{75}H_9$**, (b)** $B_{34}N_{41}H_9$-M1, **(c)** $B_{41}N_{34}H_9$-M2 (blue atoms represent nitrogen atoms and pink atoms represent boron atoms), **(d)** $Si_{34}C_{41}$ H_9-M1, **(e)** $Si_{41}C_{34}H_9$-M2 (dark cyan atoms represent silicon atoms and grey atoms represent carbon atoms).

3. Results and Discussion

3.1. Mn-Doped Nanocones

We investigate the structural stability and hydrogen storage potential of manganese-doped nanocones with varying compositions (Mn-CNCs: carbon-based, Mn-BNNCs: boron nitride-based, Mn-SiCNCs: silicon carbide-based), as depicted in Figure 3. Computational analyses reveal that nanocones with a 300° disclination angle, binding energies were computed as −148.27 eV, −161.57 eV, −151.08 eV, −182.15 eV, and −163.82 eV, for Mn-$C_{75}H_9$, Mn-$B_{34}N_{41}H_9$-M1, Mn-$B_{41}N_{34}H_9$-M2, Mn-$Si_{34}C_{41}H_9$-M1, and Mn-$Si_{41}C_{34}H_9$-M2, respectively.

Also, for nanocones with a 60° disclination angle demonstrate enhanced structural stability. Binding energy calculations for these systems yielded values of -147.27 eV, -159.86 eV, -149.9 eV, −218.29 eV, and −234.65 eV for Mn-$C_{80}H_{20}$, Mn-$B_{38}N_{42}H_{20}$-M1, Mn-$B_{42}N_{38}H_{20}$-M2, Mn-$Si_{38}C_{42}H_{20}$-M1, and Mn-$Si_{42}C_{38}H_{20}$-M2, respectively.

Stability rankings, determined by binding energy magnitudes (most negative to least negative), were established as follows: 60° disclination angle: Mn-$Si_{42}C_{38}H_{20}$-M2> Mn-$Si_{38}C_{42}H_{20}$-M1> Mn-

$B_{42}N_{38}H_{20}$-M2 > Mn-$B_{38}N_{42}H_{20}$-M1> Mn-$C_{80}H_{20}$, and for 300° disclination angle: Mn-$Si_{41}C_{34}H_9$-M2> Mn-$Si_{34}C_{41}H_9$-M1> Mn-$B_{41}N_{34}H_9$-M2> Mn-$B_{34}N_{41}H_9$-M1> Mn-$C_{75}H_9$.

These results indicate that Mn-doped silicon carbide nanocones (Mn-SiCNCs) exhibit superior stability across both disclination angles compared to their boron nitride and carbon counterparts. This trend corroborates earlier studies (El-Barbary, 2019; Savini *et al.,* 2007), underscoring Mn-SiCNCs as promising candidates for hydrogen storage applications due to their robust structural integrity.

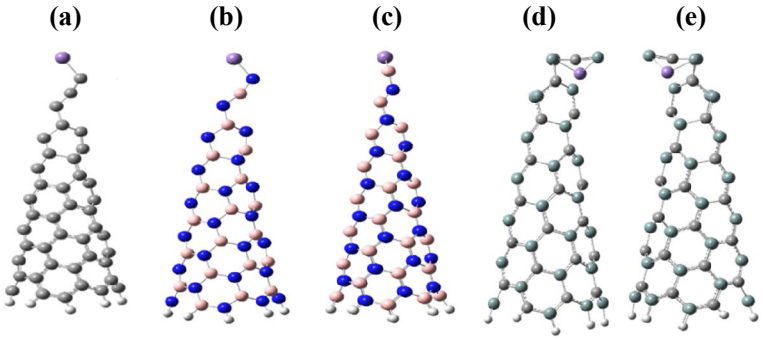

Fig. 3: The fully optimized structures of Mn-doped nanocones with disclination angle 300˚ (a) S Mn-$C_{75}H_9$, (b) Mn-$B_{34}N_{41}H_9$-M1, (c) Mn-$B_{41}N_{34}H_9$-M2 (blue atoms represent nitro gen atoms, pink atoms represent boron atoms and purple atom represent seenium atom), (d) Mn-$Si_{34}C_{41}H_9$-M1, (e) Mn-$Si_{41}C_{34}H_9$-M2 (dark cyan atoms represent silicon atoms and grey atoms represent carbon atoms).

3.2. Adsorption energy.

This research explores the potential of pure and manganese-doped nanocones (Mn-NCs) for hydrogen storage by analyzing their hydrogen adsorption characteristics. The optimized structures of Mn-doped nanocones with a 300° disclination angle are depicted in Figure 4, including configurations such as Mn-$C_{75}H_9$, Mn-$B_{34}N_{41}H_9$-M1, Mn-$B_{41}N_{34}H_9$-M2, Mn-$Si_{34}C_{41}H_9$-M1 and Mn-$Si_{41}C_{34}H_9$-M2. To quantify hydrogen adsorption, the adsorption energy ($E_{adsorption}$) was calculated using the relation:

$$\mathbf{E_{(adsorption)} = E_{(NCs\text{-}H)} - E_{(NCs)} - E_{(H)}}$$

where $E_{NCs\text{-}H}$ is the energy of the optimized hydrogenated NCs structure, E_{NCs} is the energy of an optimized pure NCs structure and E_H is the energy of a hydrogen atom. The adsorption energy for disclination angles 60˚ and 300˚ is shown in Table 1. We measure the ability of pure and doped Mn-CNCs, Mn-BNNCs and Mn-SiCNCs for hydrogen storage as a function of adsorption energy.

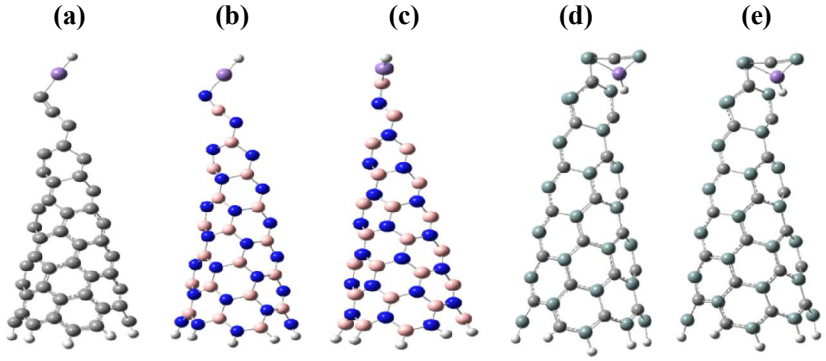

Figure 4. The fully optimized structures of hydrogen adsorption on the Se-doped nano cones with disclination angle 300˚ **(a)** Mn-$C_{75}H_9$, **(b)** Mn-$B_{34}N_{41}H_9$-M1, **(c)** Mn-$B_{41}N_{34}H_9$-M2 (blue atoms represent nitrogen atoms, pink atoms represent boron atoms and purple atom represent selenium atom), **(d)** Mn-$Si_{34}C_{41}H_9$-M1, **(e)** Mn-$Si_{41}C_{34}H_9$-M2 (dark cyan atoms represent silicon atoms and grey atoms represent carbon atoms).

Among the examined structures, the Mn-$Si_{41}C_{34}H_9$-M2 nanocone with a 300° disclination angle exhibited the strongest hydrogen binding energy (-4.98 eV), significantly outperforming its undoped counterpart $Si_{34}C_{41}H_9$-M1 (-2.38 eV). Across all Mn-doped nanocones (Mn-CNCs, Mn-BNNCs, Mn-

SiCNCs), adsorption energies were more negative than those of the undoped systems, indicating a substantial enhancement in hydrogen binding strength due to manganese incorporation as shown in Table 1. This trend aligns with previous studies on transition metal doping in graphene-based materials, including osmium- and tungsten-doped systems (Alshareef, 2020).

The exceptional adsorption performance of Mn-SiCNCs at a 300° disclination angle is attributed to their pronounced curvature and the intrinsic advantages of silicon carbide (SiC), such as high thermal conductivity, chemical stability, and favorable electronic properties. These characteristics make Mn-SiCNCs promising candidates for applications in nanocomposites, microelectronics, and optoelectronics (El-Barbary., 2019; Al-Khateeb and El-Barbary., 2020).

Table 1: The calculated adsorption energy of hydrogenated pure and doped Mn-CNCs, Mn-BNNCs and Mn-SiCNCs with disclination angles 60˚ and 300˚. All energies are given by eV.

Angle 60˚	E_{ads}^{H} **(eV)**	**Angle 300˚**	E_{ads}^{H} **(eV)**
$C_{80}H_{20}$	-1.06	$C_{75}H_9$	-1.27
Mn -$C_{80}H_{20}$	-1.74	Mn-$C_{75}H_9$	-1.95
$B_{38}N_{42}H_{20}$-M1	-1.59	$B_{34}N_{41}H_9$-M1	-1.76
Mn -$B_{38}N_{42}H_{20}$-M1	-2.15	Mn-$B_{34}N_{41}H_9$-M1	-2.38
$B_{42}N_{38}H_{20}$-M2	-1.99	$B_{41}N_{34}H_9$-M2	-2.11
Mn -$B_{42}N_{38}H_{20}$-M2	-2.63	Mn-$B_{41}N_{34}H_9$-M2	-3.87
$Si_{38}C_{42}$ H_{20}-M1	-1.83	$Si_{34}C_{41}H_9$-M1	-2.66
Mn -$Si_{38}C_{42}$ H_{20}-M1	-2.37	Mn-$Si_{34}C_{41}H_9$-M1	-3.23
$Si_{42}C_{38}H_{20}$-M2	-2.77	$Si_{41}C_{34}H_9$-M2	-3.04
Mn -$Si_{42}C_{38}H_{20}$-M2	-3.01	Mn-$Si_{41}C_{34}H_9$-M2	-4.98

3.3. Surface reactivity and energy gaps

The surface reactivity of nanostructured materials can be quantitatively assessed through dipole moment measurements, where elevated values correlate with increased chemical activity. To investigate this relationship, computational analyses were performed on undoped and manganese-doped nanocones with distinct structural geometries. Two classes of nanocones were evaluated: those with a 60° disclination angle (Mn-$C_{80}H_{20}$, Mn-$B_{38}N_{42}H_{20}$-M1, Mn-$B_{42}N_{38}H_{20}$-M2, Mn-$Si_{38}C_{42}H_{20}$-M1, Mn-$Si_{42}C_{38}H_{20}$-M2) and those with a 300° disclination angle (Mn-$C_{75}H_9$, Mn-$B_{34}N_{41}H_9$-M1, Mn-$B_{41}N_{34}H_9$-M2, Mn-$Si_{34}C_{41}H_9$-M1 and Mn-$Si_{41}C_{34}H_9$-M2).

Critical factors in nanocone device design include surface reactivity and energy gap characteristics, both of which exhibit angular dependence. As shown in Table 2, systems with a 300° disclination angle demonstrated systematically enhanced surface reactivity across carbon-based nanocones (CNCs), boron nitride nanocones (BNNCs), and silicon carbide nanocones (SiCNCs), regardless of manganese doping. For CNCs, dipole moments spanned 8.82 D (Mn-$C_{80}H_{20}$, 60°) to 18.94 D ($C_{75}H_9$, 300°). BNNCs followed analogous behavior, with Mn-$B_{42}N_{38}H_{20}$-M2 (12.54 D, 300°) and $B_{34}N_{41}H_9$-M1 (14.75 D, 300°) marking the reactivity extremes. SiCNCs displayed the most pronounced angular sensitivity, ranging from 23.62 D (Mn-$Si_{38}C_{42}H_{20}$-M1, 300°) to 25.74 D (Mn-$Si_{34}C_{41}H_9$-M1, 300°).

Table 2: The dipole moments and energy gaps of hydrogenated doped Mn-CNCs, Mn-BNNCs and Mn-SiCNCs with disclination angles 60˚ and 300˚. The dipole moment is given by Debye and the energy gap is given by eV.

Angle 60˚	Dipole Moment (Debye)	E.g (ev)	Angle 300˚	Dipole Moment (Debye)	E.g (ev)
Mn -$C_{80}H_{20}$	8.82	0.03	Mn-$C_{75}H_9$	18.94	0.04
Mn -$B_{38}N_{42}H_{20}$-M1	11.71	0.11	Mn-$B_{34}N_{41}H_9$-M1	12.54	0.01
Mn -$B_{42}N_{38}H_{20}$-M2	7.56	0.05	Mn-$B_{41}N_{34}H_9$-M2	14.75	0.04
Mn -$Si_{38}C_{42}$ H_{20}-M1	5.04	0.04	Mn-$Si_{34}C_{41}H_9$-M1	23.62	0.02
Mn -$Si_{42}C_{38}H_{20}$-M2	7.39	0.05	Mn-$Si_{41}C_{34}H_9$-M2	25.74	0.02

The angular enhancement of reactivity arises from heightened lattice strain at larger disclination angles, which destabilizes bonding networks and promotes surface interactions. Manganese incorporation amplifies this effect by introducing localized electron-rich regions (Figure 5), significantly improving hydrogen adsorption kinetics particularly in SiCNCs. These results demonstrate that synergistic manipulation of geometric strain (via disclination angle tuning) and electronic modulation (via Mn doping) can optimize nanocones for hydrogen storage applications, consistent with prior studies on defect engineering in nanostructured materials (El-Barbary, 2019; Al-Khateeb and El-Barbary, 2020; Harris, 1995; Savini *et al.,* 2007).

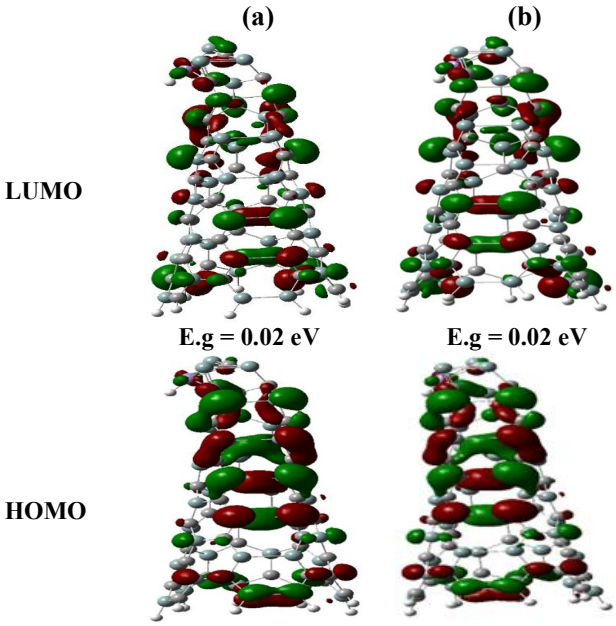

Fig. 5: The molecular orbital of LUMOs and HOMOs for hydrogenated doped Mn-SiCNCs **(a)** Mn-$Si_{34}C_{41}H_9$-M1and **(b)** Mn-$Si_{41}C_{34}H_9$-M2 with disclination angle 300˚.

3.4. Density of states.

From the total density of states DOS can be describes the number of quantum states available to electrons at each energy level in a material. It is fundamental for understanding electronic properties like conductivity and optical behavior. And from the partial density of states PDOS can be decomposes the total DOS into contributions from specific atomic orbitals or atoms, this helps identify which orbitals dominate specific energy ranges (Pantelides, 2012; Dongke Li *et al.,* 2018).

As the intensity is increased the more degeneracy is occurred. The total density of state DOS was also calculated and potted for Mn-$Si_{34}C_{41}H_9$-M1and Mn-$Si_{41}C_{34}H_9$-M2 with disclination angle 300˚.

The intensity of LUMO is higher than the intensity of HOMO for structure Mn-SiCNCs, shows that there is a significant change in Fermi level was occurred. some energy states cross Fermi level (FL), this may due to the magnetic behavior of the H-adsorbed nanocones systems. One may note that the band gap was changed upon adsorption. This observation is consistent with the change in HOMO and LUMO levels. FL lines represent Fermi Level; black line represents DOS spectra calculated by Gauss Sum. As can be seen in Figure 6.

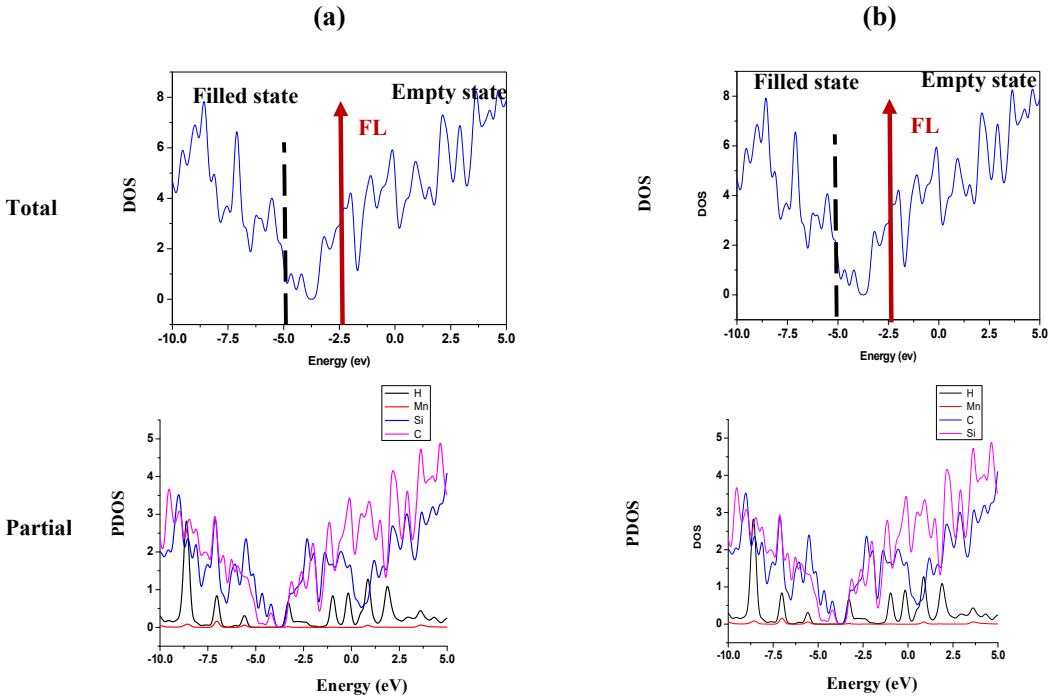

Fig. 6: The Denstiy of state and partıaı Denstiy of state with lowest energy gaps for hydrogenated doped Mn-SiCNCs **(a)** Mn-$Si_{34}C_{41}H_9$-M1and **(b)** Mn-$Si_{41}C_{34}H_9$-M2 with disclination angle 300˚.

4. Conclusion

This study presented systematic density functional theory (DFT) calculations using Gaussian 09 to investigate the hydrogen adsorption properties of pristine and manganese-doped nanocones derived from carbon, boron nitride, and silicon carbide. The findings demonstrate that both the nanocone geometry and the incorporation of transition metals critically govern adsorption behavior. Specifically, increasing the disclination angle to 300° was found to significantly enhance the interaction between hydrogen molecules and the nanocone framework. This structural effect is synergistically amplified by manganese doping, which induces a profound modification of the local electronic environment, characterized by increased surface polarization. Among the configurations examined, the Mn–$Si_{41}C_{34}H_9$–M2 nanocone with a 300° disclination angle exhibited the most favorable adsorption properties, with an adsorption energy of -4.98 eV and a concomitant surge in dipole moment to 25.74 D. These features, coupled with the narrowing of the energy gap to just 0.02 eV, signify a highly reactive electronic structure conducive to strong chemisorption. Comparative analysis further confirmed that manganese-doped silicon carbide nanocones provide markedly stronger hydrogen binding than their carbon and boron nitride counterparts. Overall, this theoretical framework underscores the powerful role of dopant-induced electronic reconfiguration and structural engineering in optimizing nanostructured materials for hydrogen capture. By identifying Mn-modified SiC nanocones as particularly promising candidates, these findings provide a rigorous foundation and valuable mechanistic insight to guide and motivate future experimental synthesis and validation, thereby bridging the gap between computational prediction and practical hydrogen storage technologies.

References

Alfieri, G. and T. Kimoto, 2009. The Structural and Electronic Properties of Chiral SiC Nanotubes: A Hybrid Density Functional Study. Nanotechnology, 20, Article ID: 285703. https://doi.org/10.1088/0957-4484/20/28/285703

Al-Khateeb, M. A. and A. EL-Barbary, 2025. Transition-Metal-Enhanced Hydrogen Adsorption on CNNCs: A DFT Analysis. Middle East Journal of Applied Sciences, 15(03), 179-188. DOI: 10.36632/mejas/2025.15.3.15.

Al-Khateeb, M. A. and A. EL-Barbary, 2026. Multiscale Investigation of Hydrogen Adsorption in Vacancy-Engineered CNCs: A Combined DFT and PHITS Monte Carlo Study. Open Journal of Composite Materials, 16(2), 59-72. https://doi.org/10.4236/ojcm.2026.162004

Al-Khateeb, M.A. and A.A. El-Barbary, 2020: Hydrogen Adsorption Mechanism of SiC Nanocones. Graphene, 9, 1-12. https://doi.org/10.4236/graphene.2020.91001

Al-Khateeb, M.A. and A.A. El-Barbary, 2018. A Theoretical Study of Hydrogen Adsorption on Surface Nanocone Materials. Current Science International, 7, 370-375. https://www.curresweb.com/csi/csi/2018/370-375.pdf

Alshareef, B., 2020. DFT Investigation of the Hydrogen Adsorption on Graphene and Graphene Sheet Doped with Osmium and Tungsten. Open Journal of Physical Chemistry, 10, 197-204. https://doi.org/10.4236/ojpc.2020.104012

Becke, A.D., 1993. Density-Functional Thermochemistry. III. The Role of Exact Exchange. Chemical Physics, 98, 5648. https://doi.org/10.1063/1.464913

Chen, P., X. Wu, J. Lin and K.L. Tan, 1999. High H2 Uptake by Alkali-Doped Carbon Nano Tubes under Ambient Pressure and Moderate Temperatures. Science, 285, 91-93. https://doi.org/10.1126/science.285.5424.91

Chen, W., Y. Zhao and Q. Sun, 2023. Transition-Metal-Decorated Graphene for Reversible Hydrogen Storage: A First-Principles Study. Journal of Physical Chemistry C, 127, 21540–21549. https://doi.org/10.1021/acs.jpcc.3c05678

Dennington, R.D., A. Frisch, T.A. Keith, J. Millam, A.B. Nielsen, A.J. Holder, and J. Hiscocks, 2009. Gauss View Manual Version 5.0.9. Gaussian Inc., Wallingford.

Dongjie, Shi, Y. Ni, G. Li, Z. Yan, Q. Zhao, W. Xie, X. Meng and J. Chen, 2022. A computational study of MgmHn nanoclusters with n:m ≥ 2:1 for efficient hydrogen storage. Institute of Applied Chemistry, 123, 7608-7617. https://doi.org/10.1002/qua.27058

Dongke, Li, J. Xu, P. Zhang, Y. Jiang and K. Chen, 2018. Transition Metal Dopants in Silicon Nanostructures. J. Phys. D: Appl. Phys. 51 233002. 51, 6463-6475. https://iopscience.iop.org/article/10.1088/1361-6463/aac1fe

EL-Barbary, A.A., 2016a. Hydrogenated Fullerenes in Space: FT-IR Spectra Analysis. AIP Conference Proceedings, 1742, Article ID: 030005. https://doi.org/10.1063/1.4953126

EL-Barbary, A.A., 2016b. Hydrogenated Fullerenes Dimer, Peanut and Capsule: An Atomic Comparison. Applied Surface Science, 369, 50-57. https://doi.org/10.1016/j.apsusc.2016.02.033

EL-Barbary, A.A., 2016c. Hydrogenation Mechanism of Small Fullerene Cages. International Journal of Hydrogen Energy, 41, 375-383. https://doi.org/10.1016/j.ijhydene.2015.10.102

El-Barbary, A.A., 201.9 Hydrogen Storage on Cross Stacking Nanocones. International Journal of Hydrogen Energy, 44, Article ID: 20099. https://doi.org/10.1016/j.ijhydene.2019.05.043

El-Barbary, A.A. and M.A. Al-Khateeb, 2021. DFT Study of Se-Doped Nanocones as Highly Efficient Hydrogen Storage Carrier. Graphene, 10, 49-60. https://doi.org/10.4236/graphene.2021.104004.

El-Barbary, A.A., K.M. Eid, M.A. Kamel, H.O. Taha, and G.H. Ismail, 2015. Ad sorption of CO, CO2, NO and NO2 on Carbon Boron Nitride Hetero Junction: DFT Study. Journal of Surface Engineered Materials and Advanced Technology, 5, 169-176. https://doi.org/10.4236/jsemat.2015.54019

El-Barbary, A.A., M.A. Kamel, K.M. Eid, H.O. Taha, R.A. Mohamed, and M.A. Al-Khateeb, 2015. The Surface Reactivity of Pure and Monohydrogenated Nanocones Formed from Graphene Sheets. Graphene, 45, 75-83. https://doi.org/10.4236/graphene.2015.4400.

El-Nahass, M.M., M.A. Kamel, A.A. El-Barbary, M.A.M. El-Mansy and M. Ibrahim, 2013. On the Spectroscopic Analyses of Thioindigo Dye. *Spectrochimica* Acta Part A: Molecular and Biomolecular Spectroscopy, 113, 332-336. https://doi.org/10.1016/j.saa.2013.05.014

Ewels, C.P., R.H. Telling, A.A. El-Barbary, and M.I. Heggie, 2003. Metastable Frenkel Pair Defect in Graphite: Source of Winger Energy. Physical Review Letters, 91, Article ID: 25505. https://doi.org/10.1103/PhysRevLett.91.025505

Frisch, M.J., Trucks, G.W., Schlegel, H.B., Scuseria, G.E., Robb, M.A., et al., 2009. Gaussian 09. Gaussian Inc., Wallingford.

Gali, A., 2006. Ab Initio Study of Nitrogen and Boron Substitutional Impurities in Single-Wall SiC Nanotubes. Physical Review B, 73, Article ID: 245415. https://doi.org/10.1103/PhysRevB.73.245415

Garberg, S.N., G. Naess, K.D. Helgesen, G. Knudsen, A. Kopstad and A. Elgsaeter, 2008. Transmission Electron Microscope and Electron Direction Study of Carbon Nanodisks. Carbon, 46, 1535-1543. https://doi.org/10.1016/j.carbon.2008.06.044

Harris, G.L., 1995. Properties of Silicon Carbide. INSPEC, the Institution of Electrical Engineers, London.

Hindi, A.A. and A.A. EL-Barbary, 2015. Hydrogen Storage on Halogenated C40 Cage: An Intermediate between Physisorption and Chemisorptions. Journal of Molecular Structure, 1080, 169-175. https://doi.org/10.1016/j.molstruc.2014.09.034

Iijima, S., 1991. Helical Microtubules of Graphitic Carbon. Nature, 354, 56-58. https://doi.org/10.1038/354056a0.

Jaramillo, D. E., H.Z.H. Jiang, H.A. Evans, R. Chakraborty, H. Furukawa, C.M. Brown, M. Head-Gordon and J.R. Long, 2021. Hydrogen Storage in Porous Cages. Journal of the American Chemical Society, 143(16), 6248–6256. https://doi.org/10.1021/jacs.1c01234

Kotz, J.C., P. Treichel, and G.C. Weaver, 2006. Chemistry and Chemical Reactivity. Thomson Brooks Cole, Pacific Grove.

Liu, C. and H.M. Cheng, 2005. Carbon Nanotubes for Clean Energy Applications. Journal of Physics D: Applied Physics, 38, 231-252. https://doi.org/10.1088/0022-3727/38/14/R01

Matsunami, H., 2004. Technological Breakthroughs in Growth Control of Silicon Carbide for High Power Electronic Devices. Japanese Journal of Applied Physics, 43, 6835. https://doi.org/10.1143/JJAP.43.6835

Nikitin, A., X.L. Li, Z.Y. Zhang, H. Ogasawara, H.J. Dai, and A. Nilsson, 200.8 Hydrogen Storage in Carbon Nanotubes through the Formation of Stable C-H Bonds. Nano Letters, 8, 162-167. https://doi.org/10.1021/nl072325k

Pakhira, S., and J. L. Mendoza-Cortes, 2019. The quantum nature in the interaction of molecular hydrogen with porous materials: implications for practical hydrogen storage. arXiv:1912.10310 (preprint). https://arxiv.org/abs/1912.10310

Pantelides, S. T., 2012. The Electronic Structure of Solids. Dynamics at Solid State Surfaces and Interfaces. 2, 1-25. https://doi.org/10.1002/9783527646463.ch1

Sattler, K., 1995. Scanning Tunneling Microscopy of Carbon Nanotubes and Nanocones. Carbon, 33, 915-920. https://doi.org/10.1016/0008-6223(95)00020-E

Savini, G., A.A. El Barbary, M.I. Heggie, and S. Öberg, 2007. Partial Dislocations under Forward Bias in SiC. Materials Science Forum, 556, 279-282. https://doi.org/10.4028/www.scientific.net/MSF.556-557.279

Shalabi, A.S., Kh. M. Eid, M.A. Kamel and A.A. El-Barbary, 1998. Comparative Study of Errors in HeH− Interaction Energy Calculations. International Journal of Quantum Chemistry, 68, 329. https://doi.org/10.1002/(SICI)1097-461X(1998)68:53.0.CO;2-X

Strobel, R., J. Garche, P.T. Moseley, L. Jorissen, and G. Wolf, 2006. Hydrogen Storage by Carbon Materials. Journal of Power Sources, 159, 781-801. https://doi.org/10.1016/j.jpowsour.2006.03.047

Suarez-Martinez, A.A. El Barbary, G. Savini, and M.I. Heggie, 2007. First-Principles Simulations of Boron Diffusion in Graphite. Physical Review Letters, 98, Article ID: 015501. https://doi.org/10.1103/PhysRevLett.98.015501

Telling, R.H., C.P. Ewels, A.A. El-Barbary, and M.I. Heggie, 2003. Wigner Defects Bridge the Graphite Gap. Nature Materials, 2, 333-337. https://doi.org/10.1038/nmat876

Vosko, S.H., L. Wilk, M. Nusair and J. Can, 1980. Influence of an Improved Local-Spin-Density Correlation-Energy Functional on the Cohesive Energy of Alkali Metals. Physical Review B, 22, 3812-3815. https://doi.org/10.1103/PhysRevB.22.3812

Wu, H., Q. Li, J. Yan and S. Yang, 2022.). High-Capacity Reversible H_2 Storage on Transition-Metal-Doped Graphene: A DFT Study. Energy & Environmental Science. 15, 2147–2159. https://doi.org/10.1039/D2EE00590A

Wu, J.J. and G.Y. Guo, 2007. Optical Properties of SiC Nanotubes: An Ab Initio Study. Physical Review B, 76, Article ID: 035343. https://doi.org/10.1103/PhysRevB.76.035343

Yang, F.H. and R.T. Yang, 2002. Adsorption Behaviors of HiPco Single-Walled Carbon Nanotube Aggregates for Alcohol Vapors. The Journal of Physical Chemistry, 106, 8994-8999. https://doi.org/10.1021/jp025767n

Yang, F.H., A.J. Lachawiec, and R.T. Yang, 2006. Hydrogen Sorption on Palladium-Doped Sepiolite-Derived Carbon Nanofibers. The Journal of Physical Chemistry B, 110, 6236-6244. https://doi.org/10.1021/jp056461u

Zeng, Y., H. Wu, and T. Xie, 2024. Hydrogen storage via adsorption: A review of recent advances and challenges. Fuel, 334, 134273. https://doi.org/10.1016/j.fuel.2024.134273

Zetterling, C.M., 2002. Process Technology for Silicon Carbide Devices. IET, Lon don. https://doi.org/10.1049/PBEP002E

Zhao, Y., Y.H. Kim, A.C. Dillon, M.J. Heben, and S.B. Zhang, 2005. Ab Initio Design of Ca-Decorated Organic Frameworks for High-Capacity Molecular Hydrogen Storage with Enhanced Binding. Physical Review Letters, 95, Article ID: 033109.

Zhu, J., Z. Yu, G.F. Burkhard, C.M. Hsu, S.T. Connor, Y. Xu, Q. Wang, M. McGe hee, S. Fan, and Y.Cui, 2009. Optical Absorption Enhancement in Amorphous Silicon Nanowire and Nanocone Arrays. Nano Letters, 9, 279-282. https://doi.org/10.1021/nl802886y